Environmental Science
Processes & Impacts

Accepted Manuscript

ROYAL SOCIETY OF CHEMISTRY

rsc.li/process-impacts

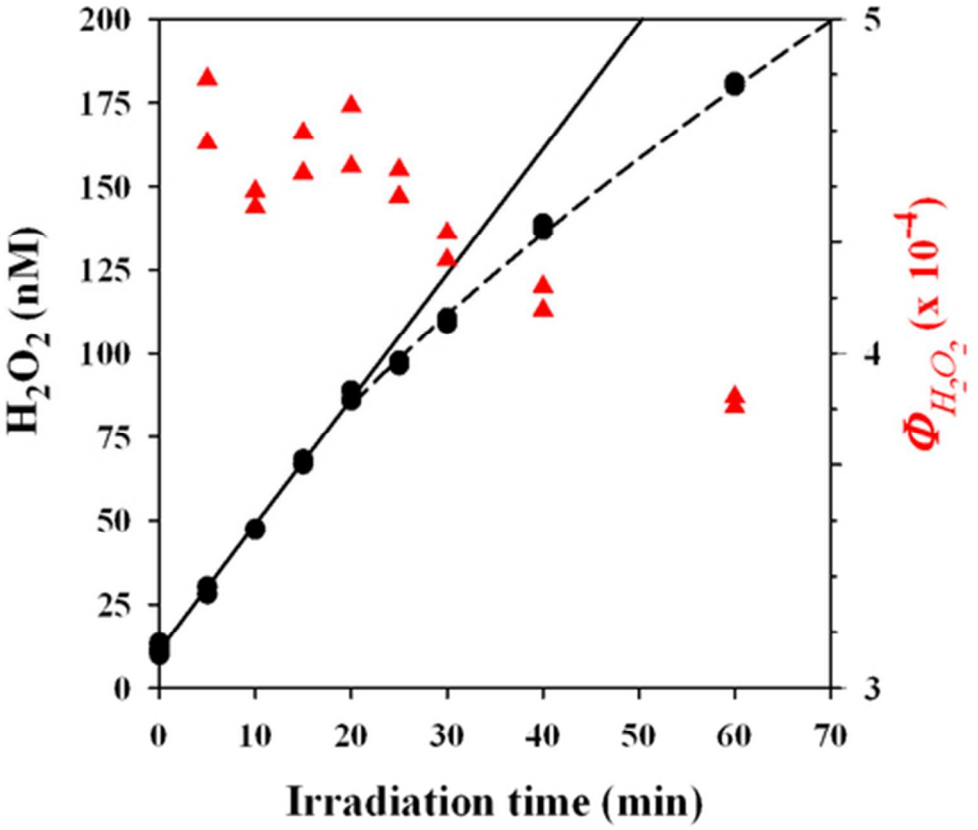

41x37mm (300 x 300 DPI)

Kieber et al. February 14, 2014

Revised Environmental Impact Statement

Photochemically produced hydrogen peroxide (H_2O_2) can negatively affect microbial activity and play an important role in many chemical reactions involving organic matter or metals in marine waters. To model production rates, wavelength and temperature dependent H_2O_2 production rates were determined as a function of absorbed irradiance (apparent quantum yields) for diverse marine environments from the Southern Ocean, Pacific Ocean, Atlantic Ocean and Gulf of Mexico. Apparent quantum yields were remarkably similar among these environments irrespective of expected differences in composition or concentrations of metals and organic matter or prior light-exposure history. The comprehensive data set for H_2O_2 apparent quantum yields reported here can be used to model H_2O_2 photochemical production rates globally based on remotely sensed optical and temperature data.

One Sentence Summary (20 word max)

Wavelength, temperature and light-dose dependent hydrogen peroxide photoproduction quantum yields were determined in subtropical, temperate and polar marine waters.

Wavelength and temperature-dependent apparent quantum yields for photochemical formation of hydrogen peroxide in seawater

David J. Kieber[1*], Gary W. Miller[1#], Patrick J. Neale[2] and Kenneth Mopper[3]

[1]State University of New York, College of
Environmental Science and Forestry,
Department of Chemistry
1 Forestry Drive
Syracuse, New York 13210

[2]Smithsonian Environmental Research Center
Photobiology and Solar Radiation Laboratory,
Edgewater, Maryland 21037

[3]Old Dominion University
Department of Chemistry and Biochemistry
Norfolk, Virginia 23529

[*]Corresponding author (djkieber@esf.edu)

#Current Address: Daiichi Sankyo Pharma Development, Edison, New Jersey 08837

Wavelength and temperature-dependent apparent quantum yields (AQYs) were determined for the photochemical production of hydrogen peroxide using seawater obtained from coastal and oligotrophic stations in Antarctica, the Pacific Ocean at Station ALOHA, the Gulf of Mexico, and at several sites along the East Coast of the United States. For all samples, AQYs decreased exponentially with increasing wavelength at 25 ^{o}C, ranging from 4.6 x 10^{-4} - 10.4 x 10^{-4} at 290 nm to 0.17 x 10^{-4} - 0.97 x 10^{-4} at 400 nm. AQYs for different seawater samples were remarkably similar irrespective of expected differences in the composition and concentrations of metals and dissolved organic matter (DOM) and in prior light exposure histories; wavelength-dependent AQYs for individual seawater samples differed by less than a factor of two relative to respective mean AQYs. Temperature-dependent AQYs increased between 0 and 35 ^{o}C on average by a factor of 1.8 per 10 ^{o}C, consistent with a thermal reaction (e.g., superoxide dismutation) controlling H_2O_2 photochemical production rates in seawater. Taken together, these results suggest that the observed poleward decrease in H_2O_2 photochemical production rates is mainly due to corresponding poleward decreases in irradiance and temperature and not spatial variations in the composition and concentrations of DOM or metals. Hydrogen peroxide photoproduction AQYs and production rates were not constant and independent of the photon exposure as has been implicitly assumed in many published studies. Therefore, care should be taken when comparing and interpreting AQY or photochemical production rate H_2O_2 results from published studies. Modeled depth-integrated H_2O_2 photochemical production rates were in excellent agreement with measured rates obtained from in situ free-floating drifter experiments conducted during a Gulf of Maine cruise, with differences (ca. 10%) well within measurement and modeling uncertainties. Results from this study provide a comprehensive data set of wavelength and temperature-

dependent AQYs to model and remotely sense hydrogen peroxide photochemical production rates globally.

1. INTRODUCTION

Hydrogen peroxide (H_2O_2) is an important species in natural waters that has been intensively studied ever since Van Baalen and Marler first quantified H_2O_2 concentrations in the Gulf of Mexico[1]. Hydrogen peroxide concentrations have been determined in a wide range of coastal and open ocean waters[2-26], wherein H_2O_2 has been shown to (1) adversely affect microorganisms at ecologically relevant concentrations[27,28]; (2) oxidize DOM through transformations involving the Fenton reaction[29,30]; (3) affect the redox chemistry of trace metals such as iron, copper, chromium and manganese[31-36]; and (4) serve as a water mass tracer for vertical advection[11,37-39].

Hydrogen peroxide concentrations vary spatiotemporally and diurnally in the oceans due to several competing processes that affect H_2O_2 concentrations in the water column. The primary removal pathway for H_2O_2 in seawater is through its biological decay[5,21,40,41]. The half-life for the biological decay of H_2O_2 in unfiltered seawater generally ranges from a few hours in coastal waters to several days in the open ocean[3,21,23,41]. Although not as important as its biological loss, photochemical decomposition of H_2O_2 has been shown to occur in sunlight surface waters at rates that were on average 5% of photochemical production rates[42].

Microorganisms remove H_2O_2 from the water column, but they are also responsible for its biological production, which is expected to occur throughout the water column[43]. A wide variety of algae and bacteria produce hydrogen peroxide and its precursor superoxide in culture[43,44], and biological H_2O_2 production has been shown to occur in oligotrophic waters under nitrogen-limiting conditions[18,45]. Biological production is the main source of H_2O_2 deeper in the water column, but in some cases may also be important in the photic zone[3,46,47]. Rain inputs are important as well[3,13,48], but they are difficult to predict and quantify. When they occur they can significantly increase H_2O_2 concentrations by a factor of 3 to 4 in the upper 20 m[8,14,49,50]. The

85 importance of rain as a source of H_2O_2 in surface waters is expected to vary with latitude, as the
86 largest rain inputs occur in the subtropics and equatorial region[6,23].

87 The primary pathway for the formation of hydrogen peroxide in sunlit surface waters is
88 through DOM photoreactions involving ultraviolet (UV) and visible (vis) solar radiation[5,51].
89 Midday photochemical production rates in marine environments are in the 1-10 nM h^{-1} range, with
90 the highest rates observed in DOM-rich coastal waters and the lowest rates observed in cooler,
91 polar waters[3,10,11,16,22,23,52]. Photoproduction of H_2O_2 is proposed to involve intramolecular
92 electron transfer reactions by excited state DOM forming radical intermediates that subsequently
93 react with dissolved molecular oxygen to form the superoxide anion, followed by its
94 disproportionation to form H_2O_2[53]. Early work suggested that 51-76% of the superoxide
95 disproportionated to form H_2O_2[41] with an uncatalyzed, second-order rate constant of 2.2 x 10^4 M^{-1}
96 s^{-1} in oligotrophic seawater, pH 8.3[54]. However, recent studies indicate that superoxide decay is
97 more complicated involving metal complexes and metal-catalyzed reactions, with a smaller
98 percentage of superoxide forming H_2O_2 than previously indicated[55-59].

99 Wavelength-dependent apparent quantum yields (AQYs) for the photochemical formation of
100 H_2O_2 have been determined in seawater[16,22,60,61] to assess the importance of UV and vis radiation
101 in H_2O_2 photoproduction[9] and to model photoproduction rates[62]. Wavelength-dependent AQYs
102 are remarkably similar in diverse marine waters[16,22,60], decreasing exponentially from ~5 x10^{-3} at
103 290 nm to ~0.1 x 10^{-4} at 400 nm, with corresponding sunlight-normalized H_2O_2 production in
104 marine waters primarily in the UV-B (280-320 nm) and UV-A (320-400 nm).

105 Building on these prior results, we conducted an extensive study to determine and compare
106 wavelength and temperature-dependent AQYs for the photochemical production of H_2O_2 in a
107 wide range of marine environments that included coastal and oligotrophic sites along the East

Coast of the United States, Gulf of Mexico, Hawaii, and Antarctica. Apparent quantum yields were used to calculate depth-integrated photochemical production rates that were compared to measured depth-integrated production rates obtained from in situ drifter experiments deployed at sea.

2. MATERIALS AND METHODS

2.1 Chemicals

Quinine sulfate dihydrate (Ultrex) and 30% aqueous H_2O_2 (Baker Analyzed, ACS reagent) were obtained from J.T. Baker. Reagent grade glacial acetic acid, hydrofluoric acid and 1,10-phenanthroline were obtained from Fisher Scientific. Certified ACS grade potassium oxalate monohydrate was obtained from Sigma-Aldrich. Certified ACS grade sulfuric acid and ferric chloride were obtained from Mallinckrodt. Certified ACS grade hydrochloric acid was purchased from VWR. Catalase (from bovine liver; 58,000 units mg protien^{-1}), tris (hydroxymethyl) amino-methane (tris), p-hydroxyphenylacetic acid (POHPAA) and horseradish peroxidase (type VI, 290 purpurogallin units mg^{-1}) were obtained from Sigma-Aldrich. The POHPAA crystals were further purified by three successive re-crystallizations from Milli-Q water. High purity, HPLC-grade methanol (MeOH) and acetonitrile (ACN) were obtained from Burdick and Jackson. The ethylene glycol used in the water baths for AQY determinations was spectrophotometric grade (>99% purity) from Sigma-Aldrich. Laboratory water (Milli-Q water) was obtained from a Millipore system consisting of a RiO8 reverse osmosis system to remove particles and chlorine and a Milli-Q Gradient system to remove trace ions and organic compounds (Millipore).

A 20 mM aqueous potassium ferrioxalate actinometer solution was prepared by adding 5 mL of 1.2 M aqueous potassium oxalate and 5 mL of 0.4 M aqueous ferric chloride to 90 mL Milli-Q

water in an aluminum foil-wrapped Qorpak bottle and sealed with a Teflon-lined cap. The 0.6 M, pH 4.5 acetate buffer solution used for the ferrioxalate actinometer was prepared in 0.18 M aqueous sulfuric acid. A 100 mL solution of 0.2% w/w 1,10-phenanthroline in Milli-Q water was prepared in subdued lab lighting and stored in an aluminum foil-wrapped Qorpak bottle. All actinometer solutions were stored at 4 ^{o}C.

The fluorometric reagent for H_2O_2 quantification was prepared by adding 0.5 mL of 25 mM purified POHPAA and 3.1 mg horseradish peroxidase to 49.5 mL of 0.25 M aqueous tris buffer (pH 8.80) in an aluminum foil-wrapped Qorpak bottle. The tris buffer, POHPAA solutions and fluorometric reagent were stored at 4 ^{o}C, and the solid horseradish peroxidase was stored at –20 ^{o}C. The fluorometric reagent blank increased with time, therefore, a fresh solution was prepared every three days. The tris and POHPAA solutions used to make the fluorometric reagent were stable and prepared as needed.

Stock solutions of H_2O_2 were prepared by adding 20 µL of 30% aqueous H_2O_2 to 20 mL Milli-Q water in a scintillation vial. The absorbance of the stock solution was measured in a 1 cm quartz cell and referenced with Milli-Q water using a Hewlett Packard 8453 UV-vis photodiode array spectrophotometer (Agilent Technologies). The concentration of the stock solution (10.1 mM) was determined spectroscopically using a molar absorptivity of 38.1 ± 1.4 M^{-1} cm^{-1} at 240 nm[63].

2.2 Hydrogen Peroxide Quantification in Seawater

Hydrogen peroxide concentrations were determined from batch fluorescence measurements of the POHPAA dimer using the method outlined in Miller and Kester[63], as modified in Yocis et al.[22], and a Hitachi F-1200 fluorometer, with the excitation and emission wavelengths set at

315±7.5 nm and 400±7.5 nm, respectively. A Rainin Rabbit Plus peristaltic pump was used to pull samples through a12 μL quartz, fluorescence flow cell using Teflon tubing (1.59 mm o.d. x 0.82 mm i.d.) and a flow rate between 0.87 to 1.0 mL min^{-1}. The fluorometer was periodically calibrated with 100 nM aqueous quinine sulfate in 0.05 M aqueous sulfuric acid. The F-1200 data were collected using E-Lab data acquisition software (OMS Tech).

To quantify H_2O_2 in seawater, a 100 μL aliquot of the fluorometric reagent was added to 5 mL seawater and reacted for 30 min followed by its fluorometric analysis. Unless otherwise noted, samples and the three blanks were analyzed in triplicate. The mV fluorescence responses recorded for the reacted seawater samples were corrected by subtracting the total blank mV response (see below). Blank-corrected responses were then used to calculate H_2O_2 concentrations by the method of standard additions. Hydrogen peroxide standards were prepared by adding μL aliquots of a 10.1 μM standard to 5.0 mL of seawater yielding concentrations between 5.0–150 nM. The detection limit of the method, 1.3 nM, was three times the standard deviation obtained from analysis of the H_2O_2 content in seven aliquots of a 0.2 μm-filtered seawater sample; the average concentration of H_2O_2 in this sample was 7.1 nM.

Three blanks were analyzed to quantify the fluorescence response of (1) seawater (NAT blank) (2) catalase (CAT blank), and (3) the fluorometric reagent (FL blank). The NAT blank was determined by measuring the fluorescence of the seawater sample without addition of the fluorometric reagent or catalase. The CAT blank was determined to allow for the determination of FL blank by reacting and removing H_2O_2 from the seawater sample. The CAT blank was determined by adding 25 μL of aqueous catalase (1.02×10^8 units catalase L^{-1}) to 5 mL of seawater in a 20 mL borosilicate vial followed by reaction for 8 min at room temperature (CAT blank). A 100 μL aliquot of fluorometric reagent was then added to the CAT blank sample and

allowed to react for an additional 30 min (FL blank). After fluorometric analysis of these three blanks, the total blank was calculated:

$$\text{total blank} = \text{NAT blank} + (\text{FL blank} - \text{CAT blank}) \quad (1)$$

All fluorescence measurements were referenced against Milli-Q water.

2.3 Seawater Sample Collection

Seawater samples were collected from stations in the confluence of the Weddell and Scotia Seas (Sta. B), along the Antarctic Peninsula at Sta. N and Arthur Harbor (Fig. 1A), and along the East Coast of the United States (Fig. 1B). The Antarctic seawater samples were collected from October 7 to November 21, 1998 during a cruise aboard the R/V *Lawrence M. Gould*. Gulf of Maine and stations E and F samples were obtained during a cruise aboard the R/V *Endeavor* from July 9 to July 27, 1999. All cruise samples were collected at 5 to 10 m with 10 L Go-Flo bottles (General Oceanics) attached to a rosette sampler equipped with conductivity, temperature and depth sensors. Seawater samples were gravity filtered directly from the Go-Flo bottles using a Whatman POLYCAP 75 AS 0.2 μm filter and stored in 4 L Qorpak bottles (capped with PTFE-lined Thermoset caps) at 4 ^{o}C until analyzed back in the home laboratory in Syracuse, NY. Prior to the cruises, the Qorpak bottles were cleaned by several rinses with MeOH and Milli-Q water followed by baking at 550 ^{o}C for 8 h. POLYCAP filters were copiously rinsed alternately with ACN and Milli-Q water until the absorbance at 220 nm and fluorescence were lowered to background levels in the Milli-Q water[64].

Seawater was also collected with a Go-Flo bottle from 5 m in the Gulf of Mexico during the summer 1998 (24^{o} 57.8′ N, 85^{o} 53.9′ W). A surface estuarine water sample was collected using an all-polypropylene bucket in the Rhode River Estuary in March 1999. These samples were

subsequently gravity filtered through a 0.2 μm POLYCAP filter into pre-cleaned 4 L Qorpak bottles. Unfiltered seawater samples were collected in 4 L Qorpak bottles from Banks Channel, North Carolina (Fig. 1B) and Station ALOHA, Hawaii (22^{o} 45.0′ N, 157^{o} 58.5′ W) during the summer 1999. These samples were filtered within two days of collection through a 47 mm diameter, 0.2 μm Nylon filter. All samples were stored in the dark at 4 ^{o}C until they were used in irradiations experiments, which were performed from less than a day to a few months after a sample was collected; most samples were analyzed within a week of sample collection.

2.4 Apparent Quantum Yields

2.4.1 ***Narrow-Bandwidth AQY Determinations*****:** To determine an AQY, a 15 mL aliquot of 0.2 μm-filtered, air-saturated seawater was placed in a 5 cm pathlength, rectangular quartz spectrophotometer cell and sealed with a Teflon-lined screw cap (Spectrocell). The quartz cell containing the seawater sample was placed into an enclosed temperature-controlled sample holder equipped with a stirrer. Prior to irradiation, the sample was equilibrated for 5 min to the sample holder temperature that was regulated with a re-circulating water-glycol bath. Since the water-glycol coolant was contained within the cell holder and did not bathe the quartz cell, the temperature inside the quartz cell was periodically verified with a thermistor. Likewise, the water-glycol coolant re-circulated through the cell holder and did not affect the narrow bandwidth radiation impingent on or passing through the 5 cm quartz cell. Sample irradiation times varied from 10 to 240 min, depending on the absorbance of the seawater, and the wavelength and temperature selected. Two 5 mL aliquots were removed from each 15 mL irradiated sample and equilibrated to room temperature before analysis. For each irradiated sample, a corresponding

dark control was also examined in the same apparatus by blocking the incoming light. Wavelength-dependent H_2O_2 production rates were converted to AQYs:

$$\Phi_\lambda = \frac{\frac{d[H_2O_2]_\lambda}{dt} V}{P_\lambda (1 - 10^{-A_\lambda})} \quad (2)$$

where Φ_λ is the wavelength-dependent AQY for H_2O_2 formation (mol (mol quanta)$^{-1}$), $d[H_2O_2]_\lambda/dt$ is the measured rate of H_2O_2 photoproduction (mol L^{-1} min^{-1}), V is volume of the irradiated seawater sample, P_λ is the spectral radiant flux (mol quanta min^{-1}) determined by ferrioxalate actinometry, and A_λ and $(1-10^{-A_\lambda})$ are the wavelength-dependent absorbance and fraction of radiation absorbed by 0.2 μm-filtered seawater in a 5 cm pathlength quartz cell, respectively. Absorbance spectra were determined from 200 to 800 nm using a 5 or 10 cm pathlength quartz cell and a Hewlett Packard 8453 UV-vis photodiode array spectrophotometer; 0.2 μm-filtered seawater sample spectra were referenced against Milli-Q water and corrected for scattering and refractive-index baseline offsets[65].

The apparatus used to irradiate seawater samples consisted of a 1 kW xenon arc lamp and LPS255HR power supply (Spectral Energy). Wavelengths were selected from 290 to 400 nm using a Spectral Energy GM 252 high intensity quarter meter grating monochromator. The lamp, monochromator and cell holder were held fixed along an optical rail so that the beam of narrow-bandwidth radiation leaving the monochromator was perpendicular to (and smaller in diameter than) the front window of the 5 cm quartz cell; the radiation passed through the front window and exited out the rear window. Unless otherwise noted, for all AQY determinations the bandwidth was set at 9.9 nm for wavelengths < 320 nm and 19.5 nm for wavelengths from 340 nm to 400 nm. For irradiations at wavelengths ≥ 360 nm, a long-pass filter with a 314 nm cut-off was placed between the monochromator and the sample holder to filter out shorter wavelengths due to

frequency doubling. The transmission spectrum for the long-pass filter is given in Miller[66]. The spectral output of the irradiation system was periodically checked using an OL754 spectroradiometer (Optronics Laboratories) that was calibrated with a 1kW NIST-traceable OL 200EA quartz-halogen lamp[66].

Temperature-dependent AQYs were determined for selected seawater samples at 290, 300, 320, 360 and 400 nm. Four temperatures (0, 15, 25 and 35 ^{o}C) were examined at each wavelength. The activation energy was calculated from linear regression analysis of the equation:

$$ln\ \Phi_\lambda = ln\ A - \frac{E_a}{RT} \quad (3)$$

where Φ_λ is the wavelength-dependent AQY, A is the pre-exponential factor, E_a is the activation energy (kJ mol^{-1}) for the formation of hydrogen peroxide, R is the universal gas constant (8.315 x 10^{-3} kJ mol^{-1} K^{-1}), and T is temperature (K).

For all laboratory AQY studies, spectral radiant fluxes were determined using the potassium ferrioxalate chemical actinometer[67,68] and the procedure outlined in White et al.[69]. Absorption values for the irradiated actinometer samples were referenced against non-irradiated potassium ferrioxalate blanks. From known ferrous production quantum yield values[68], spectral radiant fluxes (P_λ) were calculated from:

$$P_\lambda = \frac{A V_1 V_3\ 10^{-3}}{\varepsilon \Phi_\lambda\ t V_2\ L} \quad (4)$$

where A is the absorbance at 510 nm of the blank-corrected irradiated actinometer solution, V_1 is the volume of irradiated actinometer solution (15 mL), V_2 is the volume of the irradiated solution taken for spectrophotometric analysis (0.5 mL), V_3 is the final volume of the actinometer prepared for spectrophotometric analysis (10 mL), 10^{-3} is a volume conversion factor, ε is the molar absorption coefficient for ferrous phenanthroline at 510 nm (1.11 x 10^4 M^{-1} cm^{-1}), Φ_λ is

the wavelength-dependent quantum yield for ferrous iron production at wavelength λ, t is the irradiation time (min) and L is the pathlength (1 cm) of the quartz cell used to measure the absorbance of the phenanthroline complex at 510 nm.

2.4.2. *Polychromatic AQY Spectrum Determination*: In addition to wavelength-dependent AQY spectra determined with stored seawater in the laboratory in Syracuse, NY employing a narrow-bandwidth irradiation system, a wavelength-dependent AQY spectrum was also determined at the Smithsonian Environmental Research Center with freshly collected seawater using a polychromatic irradiation system described by Cullen et al.[70] and Neale and Fritz[71]. For the present study, the polychromatic irradiation system was modified to hold capped quartz vials and there were only five slots per filter treatment instead of ten as shown in Neale and Fritz[71]. Detailed diagrams and associated text for the polychromatic irradiation apparatus are presented in Neale and Fritz[71]. Briefly, the irradiation system consisted of a 2500 W Xe arc lamp with its output focused onto a mirror that redirected the polychromatic irradiation vertically 90^{o} where it passed through a panel of eight long-pass filters with cut-offs at 280, 295, 305, 320, 335, 350, 370, or 395 nm. The sample temperature was regulated to 9 ^{o}C with a re-circulating water-glycol bath; the sample temperature in each quartz cell was determined with a thermistor. A black anodized aluminum sample rack with machined cylindrical slots was placed in the water-glycol bath. Quartz vials were filled with 20 mL of 0.2 μm-filtered, air-saturated seawater, and placed into hollow black cylindrical vial holders that were threaded at the top. Each vial holder had an o-ring inserted into a groove around the inner bottom opening to hold the vial in place and seal it from the water-glycol coolant. After each quartz vial was filled with the filtered seawater sample and placed into the holder, a Teflon-lined plastic cap was screwed onto the top of the vial holder

to secure and seal the quartz vial in the vial holder. Each vial holder was then placed into a cylindrical slot in the sample rack. There were five slots above each of the eight long-pass filters. In this study, two samples were irradiated per long-pass filter treatment. After samples were placed into the aluminum rack, they were equilibrated to 9 ^{o}C prior to an irradiation. Irradiation times ranged from 15 to 360 min, depending on the spectral treatment and sample photon exposure (time-integrated irradiance[72]). Dark controls were prepared by wrapping quartz vials with black electrical tape. These controls were placed in the rack for the longest irradiation period (360 min). The spectral irradiance (mW m^{-2} nm^{-1}) was measured inside each irradiation cell (and therefore included transmission through the water-glycol bath) with a custom built fiber-optic spectroradiometer as described by Neale and Fritz[71]. Since incoming light entered the capped quartz cells vertically from the base, it was necessary to correct irradiances for scattering and multiple reflections employing nitrite chemical actinometry[73]. If this correction was not included, AQYs would be overestimated by 10-30%.

Measured H_2O_2 production rates (R_{H2O2}) were used along with irradiance data (E_λ) and wavelength-dependent sample absorbance coefficient measurements (a_λ) to determine an AQY spectrum. Measured H_2O_2 production rates were fit to:

$$R_{H2O2} = \int \Phi_\lambda \, a_\lambda \, E_\lambda d\lambda \quad (5)$$

where Φ_λ is the wavelength-dependent AQY that was determined from the AQY spectrum which was assumed to follow an exponential function:

$$\Phi_\lambda = \Phi_{300nm} \; 10^{-m_1 (\lambda - 300)} \quad (6)$$

m_1 is the slope and Φ_{300nm} is the AQY for H_2O_2 formation at 300 nm. Nonlinear regression (Marquardt algorithm) was used to estimate the m_1 and Φ_{300nm} that maximized r^2 and minimized the mean-square error between measured H_2O_2 production rates and those predicted using

equation 5[74,75]. To perform this analysis, initial boundary conditions for Φ_{300nm} and m_1 were set using the AQY and *m* determined from narrow bandwidth experiments.

2.5 Shipboard Photochemical Production Experiments

Photochemical production rates for H_2O_2 were determined during field studies in the 1998 austral spring aboard the R/V *Lawrence M. Gould* at several hydrographic stations in the confluence of the Weddell and Scotia Seas as well as along the Antarctic Peninsula. Production rates were also determined at stations in the Gulf of Maine and North Atlantic Ocean during the 1999 summer aboard the R/V *Endeavor*. Production rates were determined in the field with freshly collected seawater samples in order to compare to modeled rates that were determined using AQY results obtained with stored seawater in the home laboratory. Hydrogen peroxide production rates were determined at sea using the procedures described in Yocis et al.[22] and Teflon-sealed quartz irradiation vessels[76] filled with 0.2 μm-filtered, air-saturated seawater.

2.5.1. *Wavelength-Dependent H_2O_2 Production Rates*: Shipboard experiments were conducted to determine the photochemical production of H_2O_2 in the UV-B (290-320 nm), UV-A (320-400 nm), and visible region of the solar spectrum. Duplicate quartz tubes were placed in a flow-through surface seawater bath and exposed to sunlight on the ship's aft deck between 10:00 and 16:00 local time. Details of the quartz tube design are given in Kieber et al.[76]. Production rates for H_2O_2 in these quartz tubes were compared to rates determined in quartz tubes that were wrapped in Mylar D polyester film or placed in a UF3 Plexiglas box. Mylar D polyester film and UF3 Plexiglas cut-off wavelengths were 313 and 400 nm, respectively (Fig. 2).

2.5.2. *In Situ H_2O_2 Production Rates*: Depth-dependent, daytime H_2O_2 production rates were determined by placing duplicate quartz tubes at six depths from 2 to 20 m using a free-floating drifter described by Kieber et al.[76]. The daytime production rate was also determined at the sea surface in a flow-through seawater bath on the aft deck of the R/V *Endeavor* in a location with minimal shading. The free-floating drifter and surface samples were deployed prior to sunrise (ca. 05:00) and retrieved after sundown (ca. 20:00) to obtain average daily photochemical production rates for hydrogen peroxide as a function of water-column depth. Controls were examined to determine hydrogen peroxide production during the deployment and retrieval of the drifter[22]. Experimentally determined in situ production rates were compared to calculated depth-integrated, daily production rates:

$$R_{H2O2} = \iiint \Phi_{T,\lambda} a_{z,\lambda} E_{z,\lambda,t} dz d\lambda dt \quad (7)$$

where R_{H2O2} is the depth- (z) and wavelength-integrated, daytime production rate, $\Phi_{T,\lambda}$ is the temperature- and wavelength-dependent AQY, a_λ is the wavelength- and depth-dependent CDOM absorption coefficient, and $E_{z,\lambda,t}$ is the wavelength-, depth- and time-dependent spectral irradiance, and $d\lambda$ is the wavelength bandwidth (1 nm). R_{H2O2} was calculated every 0.5 m (dz) from 0 to 20 m. The spectral irradiance ($E_{z,\lambda}$) at depth z was determined from:

$$E_{z,\lambda} = E_{0,\lambda} e^{-K_{z,\lambda} z} \quad (8)$$

where $E_{0,\lambda}$ is the spectral irradiance at the sea surface and $K_{z,\lambda}$ is the wavelength-dependent downwelling attenuation coefficient. $K_{z,\lambda}$ was determined from linear regression analysis of ln $E_{z,\lambda}/E_{0,\lambda}$ versus depth. Underwater irradiance measurements were made to determine $K_{z,\lambda}$ using a NIST-calibrated free-falling Profiling Multi-Channel Radiometer (Satlantic, Inc., Halifax, Nova Scotia) that measured the irradiance at thirteen spectral channels: 304, 323, 338, 380, 411, 442, 489, 510, 523, 555, 670, 683, and 700 nm. The bandwidth for each channel was 10 nm. The

Satlantic Radiometer was deployed from the aft winch and allowed to free fall after it was situated approximately 30-60 m from the stern of the ship; several down casts were averaged to determine the spectral irradiance as a function of depth. Surface irradiance measurements were made every 15 min from 290 to 600 nm at 1 nm intervals with an NIST-calibrated Optronics Laboratories OL 754 spectroradiometer. Integrating surface irradiance measurements with time yielded $E_{0,\lambda,t}$; $E_{z,\lambda,t}$ were calculated using $E_{0,\lambda,t}$ and $K_{z,\lambda}$.

3. RESULTS AND DISCUSSION

3.1 Reciprocity for H_2O_2 Photoproduction

Experiments were conducted employing the narrow bandwidth irradiation system to determine if hydrogen peroxide production was a linear function of the photon exposure. For all wavelengths examined, H_2O_2 formation was initially a linear function of photon exposure. As an example, H_2O_2 production was linear from 0 to 20 min at 300 nm for a coastal seawater sample collected from the Gulf of Maine at Ammen Rock (Fig. 3). The photoproduction of H_2O_2 was non-linear for irradiations longer than approximately 25 min at 300 nm (Fig. 3) even though there was very little change in CDOM absorbance (< 5%). Several factors can result in this non-linear behavior, but the fact that the CDOM absorbance changed very little in these experiments indicated that the non-linearity was likely due to the loss of specific precursors leading to the formation of H_2O_2 or the loss of H_2O_2 (at the shorter wavelengths) through its direct or indirect photolysis[42]. This non-linearity resulted in an approximately 15% decrease in the AQY between 25 and 60 min. A lack of reciprocity over short time scales was unexpected and may partly explain the subsurface maximum in average, net daytime hydrogen peroxide photoproduction rates that were observed in two in situ irradiation experiments conducted in the confluence of the

Weddell and Scotia Seas[22]. These subsurface production rate maxima may have resulted from greater photon exposures in the near surface samples, especially in the UV, that reduced production rates at these depths due to non-reciprocity, whereas reciprocity may have been met for samples incubated deeper in the water column giving rise to slightly higher production rates at intermediate depths.

Lack of reciprocity was not only observed at 300 nm and was not limited to the Ammem Rock sample. Similar results were obtained for other seawater samples and at other wavelengths, although for longer wavelengths reciprocity occurred over much longer time frames (e.g., 6 h at 400 nm). All AQYs were determined in this study within the linear portion of the production plot where reciprocity was observed. Under these conditions, AQYs should be constant and not a function of photon exposure. Except for a few cases[78,79], reciprocity is rarely tested in natural-water photochemical studies when AQYs are determined. Nonetheless, in nearly all cases where H_2O_2 concentrations have been determined as a function of photon exposure using sunlight or a Xe-lamp (or Hg-lamp) based irradiation system, it has been shown that H_2O_2 accumulation is non-linear after exposures between 20 to 120 min (and in some cases even as short as 5 min) in a range of freshwater and marine samples[78,81-84] and aqueous solutions of organic matter isolates[17,53,85]. Non-linear H_2O_2 accumulation rates imply that corresponding AQYs would decrease as well if CDOM absorbance coefficients photobleached more slowly than H_2O_2 accumulation rates decreased. Therefore, care should be taken in reporting, comparing and interpreting AQYs, and photochemical production or loss rates for indirect photochemical processes in seawater, since rates will not be a linear function of photon exposure upon long-term irradiation as has been implicitly assumed in many published studies.

3.2 Comparison of Polychromatic and Narrow Bandwidth AQY Spectra

An experiment was conducted with 0.2 μm-filtered Rhode River estuary water (salinity 11.1 ppt) to compare the wavelength-dependent AQY spectrum determined using the polychromatic irradiation system to that obtained with the narrow bandwidth irradiation system. Apparent quantum yields that were determined with the polychromatic and narrow bandwidth irradiation systems were in good agreement at all wavelengths that were examined (Fig. 4). For both approaches, AQY spectra decreased exponentially with increasing wavelength, and no localized maxima or minima were noted in the narrow-bandwidth generated AQY spectrum. When the polychromatic and narrow bandwidth spectra were compared to each other, the largest differences in AQYs ($\leq$ 20%) were observed at wavelengths between 320 and 360 nm. For example, at 320 nm the average AQY determined by narrow bandwidth radiation was 2.0×10^{-4} compared to 2.4×10^{-4} determined with polychromatic radiation; this difference was not significant at the 95% confidence interval as was the case for comparisons at other wavelengths. The close agreement between polychromatic and narrow-bandwidth based AQY spectra indicated that there were no significant polychromatic wavelength interactions that affected AQYs. In other words, an AQY determined at one wavelength (e.g., 350 nm) by either narrow-bandwidth or polychromatic irradiations was not affected by irradiations at shorter (e.g., <340 nm) or longer (e.g., >360 nm) wavelengths. These results confirm the suitability of applying an exponential function to phenomenologically describe H_2O_2 AQY spectra in marine waters. Given the good agreement between these two approaches in determining AQYs for H_2O_2 photoproduction, it would be advantageous to determine AQYs using the polychromatic irradiation system because AQY spectra can be obtained in a fraction of time (e.g., day) required to determine AQY spectra using a narrow-bandwidth irradiation system (e.g., week). Furthermore, our results validate the use of

narrow-bandwidth determined H_2O_2 photoproduction AQY to model H_2O_2 photochemical production rates in natural waters that are exposed to polychromatic solar radiation.

In a separate experiment, the 0.2 μm-filtered Rhode River estuary water was stored for 2.5 months at 4 ^oC, and wavelength-dependent AQYs were determined using the narrow bandwidth irradiation system to determine the effect of sample storage on AQYs. Apparent quantum yields did not change compared to initial wavelength-dependent AQY values determined with the freshly collected water (no significant difference noted at the 95% confidence level employing a two-tailed t test) demonstrating that there were no significant changes in AQYs due to long-term, cold storage in the dark (Fig. 4). The same result was seen in CDOM spectra (i.e., no changes were seen after 2.5 months, data not shown).

3.3 Wavelength-Dependent AQYs

Wavelength-dependent AQYs for the photochemical formation of hydrogen peroxide were determined at 25 ^oC in 0.2 μm-filtered seawater samples collected from Booth Bay Harbor, Ammen Rock, Rhode River estuary, Banks Channel, Gulf of Mexico, Station ALOHA, and Antarctic stations B, N and Arthur Harbor. For all seawater samples, AQYs decreased exponentially with increasing wavelength, ranging from 3.6×10^{-4} - 10.4×10^{-4} at 290 nm to 0.17×10^{-4} - 0.97×10^{-4} at 400 nm (Fig. 5). A tabular listing of all AQYs determined at 25 ^oC is given in Miller[66]. Surprisingly, wavelength-dependent AQYs for individual seawater samples differed by less than a factor of two relative to mean AQYs determined by non-linear regression analysis of all the AQY data for all seawater samples that were examined in this study (Fig. 5). In addition, comparison of AQYs from different seawater samples shown in Fig. 5 indicated that there was no clear trend that would suggest that AQYs were higher or lower for coastal stations

compared to oligotrophic stations. It is remarkable how similar wavelength-dependent AQYs are among the different water samples even though the concentrations and speciation of metals and sources and concentrations of DOM giving rise to H_2O_2 photoformation are presumably different (e.g., terrestrial vs. marine), and the samples will have had different light-exposure histories. Given the similarity in wavelength-dependent AQYs among the seawater samples that were examined in this study, data were combined to yield an AQY spectrum (see best-fit line in Fig. 5, equation 9) that was derived from non-linear regression analysis of the composite AQY data set; this equation can be used to estimate wavelength-dependent AQYs for H_2O_2 photoproduction at 25 ^{o}C:

$$\Phi_\lambda = 1.70\, e^{-0.0272\,\lambda} \quad (9)$$

The slope (±95% confidence interval) of this line, -0.0272 ± 0.0014 nm^{-1}, is not statistically different from the slope (-0.0267 ± 0.0028 nm^{-1}) reported by Yocis et al.[22] using pooled AQY data from the Caribbean Sea, Orinoco River outflow (Venezuela), Suwanee River (GA), Vineyard Sound (MA), Shark River outflow (FL), and the Antarctic. This provides further evidence that AQYs are similar in all marine waters tested to date irrespective of expected differences in local DOM composition and light history. However, this finding may not extend to some terrestrially-dominated freshwater or ground water systems where a few relatively high AQYs have been reported[4,61,81].

3.4 Temperature-Dependent AQYs

Temperature dependence studies were conducted with seawater from Booth Bay Harbor, Rhode River estuary, Station ALOHA, and Antarctic stations B, N and Arthur Harbor. As evident from the example Arrhenius plots shown in Fig. 6, AQYs decreased with decreasing

473 temperature for all seawater samples and all wavelengths that were examined. On average, AQYs
474 decreased by a factor 1.8 per 10 ^{o}C. A tabular listing of temperature-dependent AQYs is given in
475 Miller[66].

476 Activation energies for the photochemical production of H_2O_2 in seawater determined from
477 linear regression analysis of the Arrhenius plots ranged from 8.3 to 52.7 kJ mol^{-1} (Table 1). For
478 all water samples tested, E_a increased with increasing wavelength (Table 1, Fig. 7). The largest
479 difference in the E_a was seen for the Antarctic seawater sample collected from Antarctic Station
480 B, which had a lower E_a at 290, 300 and 320 nm compared to the other samples including two
481 other Antarctic waters (Sta. N and Arthur Harbor). Likewise, for all samples, the largest
482 difference was observed when comparing E_a at 290 to 400 nm, where the average value for E_a
483 increased from 16.6 to 31.9 kJ mol^{-1}. Our average E_a determined at 400 nm, 31.9 $\pm$ 12 kJ mol^{-1}
484 (Fig. 7) agreed well with the $\geq$ 365 nm E_a value of 37.4 kJ mol^{-1} determined by Szymczak and
485 Waite[78]. In their study, they used a 365 nm band-pass filter and a Hg lamp to determine E_a for the
486 photochemical formation of H_2O_2 in an estuarine sample near the mouth of Port Hacking River
487 Estuary. This E_a included the temperature dependence for H_2O_2 photoformation not only for the
488 365 nm Hg emission line but also from several strong emission lines greater than 400 nm
489 including ones at 405 and 436 nm.

490 Although differences were observed in our study in E_a among samples and as a function of
491 wavelength, overall differences were not large except in a few cases. Therefore, for the purpose
492 of aiding modeling efforts, we determined the average E_a between 300 and 370 nm where E_a
493 differences among samples and wavelengths were relatively small, and this wavelength range
494 encompasses the main spectral H_2O_2 photoproduction bandwidth observed in coastal and
495 oligotrophic seawater based on published spectra[16,22] and results presented here. Within this UV

bandwidth, E_a for H_2O_2 photoproduction were the same for all samples tested within the 95% CI (except for Arthur Harbor, Antarctica), with a mean value of 21.8 kJ mol^{-1}. Using this mean activation energy, the temperature dependence for $\Phi_{\lambda,T}$ was determined from:

$$ln\frac{\Phi_{\lambda,T}}{\Phi_{\lambda,298}} = \frac{21.8}{R}\left(\frac{1}{298} - \frac{1}{T}\right) \quad (10)$$

where $\Phi_{\lambda,298}$ is the wavelength-dependent AQY at 298 K calculated from equation 9.

The increase in activation energies between 290 and 400 nm (Table 1) and the factor of 1.8 increase in the average AQY per 10 ^oC increase in temperature are consistent with a thermal process controlling the formation of hydrogen in seawater. Likely rate-limiting reactions controlling production are the uncatalyzed[54] and catalyzed[55-59,86-89] thermal disproportionation reactions to form H_2O_2. These reactions are complex and not fully resolved[87]. Our results suggest that the relative importance of the different disproportionation reactions may vary with wavelength, due to changes in associated light-driven reactions, which in turn may lead to wavelength-dependent changes in E_a. It is also possible that the branching ratio for catalyzed O_2^- dismutation versus non-dismutation decay pathways for O_2^- involving metals or DOM[58,78, 87,91] may vary with wavelength, thereby affecting observed E_a values. Despite uncertainties regarding why E_a increases with increasing wavelength of irradiation, the fact that E_a does change with wavelength and between water samples indicates that there are some very interesting wavelength-dependent changes in the main pathways leading to H_2O_2 photoformation in natural waters that warrant further research.

3.5 Sunlight-Normalized H_2O_2 Production Rates

Sunlight normalized production rates for hydrogen peroxide at the sea surface are shown in Fig. 8 for two coastal and two oligotrophic seawater stations. Spectrally-resolved, sunlight-

519 normalized rates (i.e., the product of $E_\lambda a_\lambda \Phi_\lambda$) were calculated at 1 nm intervals from 290 to 500
520 nm. Spectral irradiance data were obtained from Optronics spectroradiometer measurements
521 made every 15 min at the Damariscotta River outflow station on a cloudless day, July 20, 1999.
522 The mean response wavelength for hydrogen peroxide photoproduction at the sea surface was
523 determined by integrating the area under each curve in Fig. 8 between 290 and 500 nm and
524 calculating the wavelength corresponding to half the area. Based on this calculation, the mean
525 response wavelengths for the four stations were 330 nm for Ammen Rock, 322 nm for the Rhode
526 River estuary, 318 nm for Station ALOHA, and 322 nm for Antarctic Station N (Fig. 8). In
527 addition to the mean response wavelength, the response bandwidth was also determined. The
528 response bandwidth, defined as the width at half-height of the response curve, varied from 302-
529 335 nm for the Rhode River estuary, 301-333 nm for Station ALOHA, 302-335 nm for Antarctic
530 Station N, to 303-346 nm for the Gulf of Maine, Ammen Rock Station (Fig. 8). Other than a
531 slight red shift in the sunlight-normalized spectrum at Ammen Rock, these dissimilar samples had
532 nearly the same spectral shape and peak response wavelength. Peak responses and spectral
533 shapes were also quite similar to that observed for several other species that are photochemically
534 formed or removed from seawater including dimethylsulfide[64,92,93], carbonyl sulfide[94] and
535 ammonia[95], even though the processes leading to the production or loss of these compounds are
536 undoubtedly quite different. However, not all compounds show the same spectral shape and peak
537 response including (1) dissolved molecular oxygen whose spectrally-dependent photochemical
538 loss is quite broad spanning the UV and extending into the blue portion of the solar spectrum[79],
539 (2) formaldehyde photoproduction that is initiated by UV-B solar radiation[96] and (3) DIC and CO
540 photoformation rates that are red shifted with a significant contribution at wavelengths greater
541 than 400 nm[69,97]. None of these differences are surprising, as they reflect fundamentally different

reactants, photosensitizers and pathways leading to the formation or loss of these different compounds.

The importance of UV in controlling H_2O_2 photoproduction was also evident from integrating the area under the curve for each seawater sample in Fig. 8; 29-51% of the total photoproduction was in the UV-B, 48-63% was in the UV-A and only a small fraction, 1-9%, was greater than 400 nm. This finding is in good agreement with the Gulf of Maine and Palmer Station field studies where H_2O_2 production rates determined in quartz tubes were compared to production rates in Mylar-wrapped quartz tubes and quartz tubes enclosed in UF3 Plexiglas (Fig. 9). These plastic coverings approximated UV-B and total UV (< 400 nm) exclusion filters, respectively. Based on differences in H_2O_2 photoproduction between the different treatments, 38-52, 45-47 and 4-16% of the total H_2O_2 production was observed in the UV-B, UV-A and > 400 nm, respectively, in the Gulf of Maine samples; and 32, 64 and 3% was observed in the UV-B, UV-A and > 400 nm, respectively, in seawater collected from Arthur Harbor, Palmer Station, Antarctica. These field results obtained with freshly collected and 0.2 μm-filtered samples agreed well with the relative trends observed in our lab-based results with stored 0.2 μm-filtered seawater samples indicating that sample storage did not significantly affect samples with respect to H_2O_2 photoproduction.

3.6 In Situ and Modeled H_2O_2 Photoproduction Rates

During the 1999 Gulf of Maine cruise, a free-floating drifter[76] was deployed to measure total daytime photochemical production rates for hydrogen peroxide as a function of depth at the coastal stations Ammen Rock and the Damariscotta River outflow, and at the oligotrophic station E in the northwest Atlantic Ocean (Fig. 1B). For all free-floating drifter studies, total daytime photochemical production rates for H_2O_2 were highest at the sea surface and decreased

exponentially with increasing depth (Fig. 10). Mean surface photochemical production rates determined at the two coastal stations, 207 and 277 nM d^{-1}, were approximately three times greater than at the oligotrophic station E (72 nM d^{-1}). Production rates at the two coastal stations decreased rapidly below the sea surface to 2.7 and 9.9 nM d^{-1}, respectively, at 15 m, whereas rates at Station E in the northwest Atlantic Ocean (Fig. 1B) decreased more slowly with depth to 24 nM d^{-1} at 15 m. Differences in the vertical attenuation of production rates in the water column observed between the coastal and oligotrophic stations were consistent with differences in downwelling attenuation coefficients, K_d, among these stations. In particular, solar radiation was attenuated in the water column much faster at the coastal stations compared to the oligotrophic station E, especially at the shorter wavelengths in the UV. For the Damariscotta River outflow and Ammen Rock stations, K_d at 323, 338 and 411 nm were 1.5, 1.0, and 0.43 m^{-1}, and 0.70, 0.56 and 0.21 m^{-1}, respectively, whereas K_d values at Station E were considerably smaller at 0.19, 0.09 and 0.04 m^{-1}, respectively. Likewise, vertical attenuation of H_2O_2 production rates in the water column (see Yocis et al.[22] for details regarding this calculation) were 0.32, 0.20, and 0.07 m^{-1} for the Damariscotta River outflow, Ammen Rock and Station E, respectively, paralleling differences in K_d among these stations (i.e., lower K_d values corresponded to lower photochemical attenuation rates).

Since reciprocity was not met for fairly short irradiations (ca. 20-60 min) of Ammen Rock seawater (Fig. 3) and given the length of the drifter studies (ca. 05:00-20:00 local time), it is not surprising that day-long exposure of Ammen Rock seawater to solar radiation in the drifter study (Fig. 10A) led to 41% lower observed daytime rates in the near-surface exposed samples compared to modeled rates determined from equation 7. This near-surface difference was not observed in the Damariscotta River outflow drifter study (Fig. 10B), perhaps due to the faster

attenuation of UV in the water column at this station (as evidenced by larger K_d values) compared to the Ammen Rock station. Lower than expected in daily rates observed at Ammen Rock and in the Antarctic[22] in near surface waters may represent the norm, as there is no reason to expect that production rates should be constant with increasing light dose in a natural setting, especially near the sea surface. This lack of reciprocity, as evidenced by lower rates, will be an issue when comparing results from different studies when solar (or solar simulator) exposure times are significantly different or when applying AQYs to model daily rates.

Deeper in the water column ($\geq$ 4 m), modeled rates underestimated in situ rates from 30 to 90%, but these differences are more likely due to uncertainties in the parameters (Φ_λ, a_λ, $K_{d,\lambda}$, $E_{z,\lambda}$) used in the model[98] and variability in observed rates as opposed to "real" differences between the model and observations. For example, uncertainties for modeled wavelength-dependent AQYs ranged from 27% at 290 nm to 12% at 400 nm. In addition, absorption coefficients, irradiances and downwelling attenuation coefficients had errors ranging from < 1 to > 100%, depending on the wavelength and depth in the water column. Using estimates for wavelength-dependent errors for each of these parameters, propagation of error analysis was conducted to determine the coefficient of variation of wavelength-dependent production rates for each depth. The coefficient of variation of modeled production rates for the two drifter deployments ranged from 4-5% at the surface, 8-13% at 2 m, 14-25% at 4 m, 22-44% at 6 m, 31-64% at 8 m, 39-103% at 10 m and 60-450% at 15 m. This error analysis did not take into account errors associated with surface seawater reflection or changes in CDOM absorption (we assumed 100% radiative transfer and constant CDOM absorbance—i.e., no photobleaching), which would further increase modeling uncertainties.

Despite uncertainties in our photochemical model, modeled depth-integrated production rates between 0 and 20 m at Ammen Rock and the Damariscotta River outflow differed from measured depth-integrated rates over the same depth interval by only 9 and 14%, respectively (Table 2), and any differences noted at a given depth (as previously discussed) cancelled out when rates were integrated vertically in the upper 20 m. In addition, although surface production rates at the oligotrophic Station E in the northwest Atlantic Ocean were much lower than at the coastal stations in the Gulf of Maine, depth-integrated production rates were nearly the same at all three stations (Table 2) because H_2O_2 was produced at greater depths at Station E relative to the coastal stations (Figure 10). Yocis et al.[22] observed that the depth-integrated production rate at an oligotrophic station, Crystal Sound, Antarctic was almost twice the rate at a coastal Antarctic seawater station undergoing a *Cryptomonas* bloom. These comparisons demonstrate the importance of oligotrophic waters in H_2O_2 photoproduction, and more broadly illustrate the importance of considering the entire photochemically-active water column in assessing the importance of a photoprocess in marine waters.

4. CONCLUSIONS

The main finding of this study is that, although differences are observed, wavelength-dependent AQYs for the photochemical formation of H_2O_2 in seawater are remarkably similar among diverse marine environments that presumably contain varying composition and concentrations of metals and DOM from a range of terrestrial and marine sources and that have different light-exposure histories. Thus, the question arises: Why are wavelength-dependent AQYs for H_2O_2 production in Antarctic waters so close in value to wavelength-dependent AQYs determined in estuarine water from Banks Channel, NC? Perhaps AQY are similar because

633 marine DOM, despite expected source differences, is reworked by marine microorganisms
634 yielding a similar reservoir of DOM or metal-DOM complexes that serve as photochemical
635 precursors for superoxide formation or as catalysts for O_2^- dismutation and H_2O_2 formation.
636 Results presented in this study provide the data needed to model H_2O_2 production rates in
637 seawater on a global scale using remotely sensed CDOM absorbance, sea-surface spectral
638 irradiance and sea-surface temperature data, as was done in a companion paper[55]. For future
639 studies it will be important to investigate the assumption that AQYs are constant as a function of
640 photon exposure not only for H_2O_2 production but for other compounds as well (e.g., DIC, CO,
641 DMS, COS, acetaldehyde). If AQY vary with photon exposure as suggested by our results, then
642 it will be important to assess the ramifications of these findings to remotely sensed production or
643 loss rate estimates or for conclusions regarding carbon cycling in marine waters based on
644 relatively short photochemical exposure experiments[99]?
645

646 **ACKNOWLEDGMENTS**

647 We gratefully acknowledge the officers and crew of the R/V *Nathaniel B. Palmer*, the R/V *L. M.*
648 *Gould*, and the R/V *Endeavor*. We also thank the Antarctic Support Associates, and Agencias
649 Universales S.A. for their logistical support during the 1997 and 1998 Antarctic field studies, and
650 the National Science Foundation for financial support to DJK (OPP-9610173 and OCE-9711174)
651 and KM (OPP-9527255 and OCE-9711206). Thanks are also extended to Drs. Robert Kieber
652 (University of North Carolina), and David Karl (University of Hawaii) for water samples; Dr.
653 William L. Miller (University of Georgia) for light attenuation data obtained during the Gulf of
654 Maine cruise; and Dr. Jennifer Fritz (Rosenstiel School for Marine and Atmospheric Science) for

polychromatic irradiance data. Thanks are also extended to two anonymous reviewers for their thorough and thoughtful comments that improved the clarity and quality of this manuscript.

REFERENCES

1 C. Van Baalen and J. E. Marler, Occurrence of Hydrogen Peroxide in Sea-Water, *Nature*, 1966, **211**, 951.

2 D. Abele-Oeschger, H. Tüg and R. Röttgers, Dynamics of UV-Driven Hydrogen Peroxide Formation on an Intertidal Sandflat, *Limnol. Oceanogr.*, 1997, **42**, 1406-1415.

3 G. B. Avery Jr., W. J. Cooper, R. J. Kieber and J. D. Willey, Hydrogen Peroxide at the Bermuda Atlantic Time Series Station: Temporal Variability of Seawater Hydrogen Peroxide, *Mar. Chem.*, 2005, **97**, 236– 244.

4 W. J. Cooper, R. G. Zika, R. G. Petasne and J. M. C. Plane, Photochemical Formation of H_2O_2 in Natural Waters Exposed to Sunlight. *Environ. Sci. Technol.*, 1988, **22**, 1156-1160.

5 W. J. Cooper, C. Shao, D. R. S. Lean, A. S. Gordon and F. E. Scully, Factors Affecting the Distribution of H_2O_2 in Surface Waters, in *Environmental Chemistry of Lakes and Reservoirs*, ed. L. A. Baker, American Chemical Society, Washington DC, 1994, pp 391-422.

6 P. L. Croot, P. Streu, I. Peeken, K. Lochte and A. R. Baker, Influence of the ITCZ on H_2O_2 in Near Surface Waters in the Equatorial Atlantic Ocean, *Geophys. Res. Lett.*, 2004, **31**, L23S04, doi:10.1029/2004GL020154.

7 P. L. Croot, P. Laan, J. Nishioka, V. Strass, B. Cisewski, M. Boye, K. R. Timmermans, R. G. Bellerby, L. Goldson, P. Nightingale and H. J. W. de Baar, Spatial and Temporal Distribution of Fe(II) and H_2O_2 During EisenEx, an Open Ocean Mescoscale Iron Enrichment, *Mar. Chem.*, 2005, **95**, 65-88.

8 A. K. Hanson, N. W. Tindale and M. A. R. Abdel-Moati, An Equatorial Pacific Rain Event: Influence on the Distribution of Iron and Hydrogen Peroxide in Surface Waters, *Mar. Chem*., 2001, **75**, 69-88.

9 K. Fujiwara, T. Ushiroda, K. Takeda, Y. -I. Kumamoto and H. Tsubota, Diurnal and Seasonal Distribution of Hydrogen Peroxide in Seawater of the Seto Inland Sea, *Geochem. J.*, 1993, **27**, 103–115.

10 L. J. A. Gerringa, M. J. A. Rijkenberg, K. R. Timmermans and A. G. J. Buma, The Influence of Solar Ultraviolet Radiation on the Photochemical Production of H_2O_2 in the Equatorial Atlantic Ocean, *J. Sea Res.*, 2004, **51**, 3-10.

11 K. S. Johnson, S. W. Willason, D. A. Wiesenburg, S. E. Lohrenz and R. A. Arnone, Hydrogen Peroxide in the Western Mediterranean Sea: A Tracer for Vertical Advection, *Deep-Sea Res*., 1989, **36**, 241-254.

12 R. J. Kieber and G. R. Helz, Temporal and Seasonal Variations of Hydrogen Peroxide Levels in Estuarine Waters, *Estuar. Coast. Shelf Sci*., 1995, **40**, 495-503.

13 R. J. Kieber, W. J. Cooper, J. D. Willey and G. B. Avery, Hydrogen Peroxide at the Bermuda Atlantic Time Series Station. Part I: Temporal Variability of Atmospheric Hydrogen Peroxide and Its Influence on Seawater Concentrations, *J. Atm. Chem.*, 2001, **39**, 1– 13.

14 W. L. Miller and D. R. Kester, Peroxide Variations in the Sargasso Sea, *Mar. Chem.*, 1994, **48**, 17-29.

15 G. W. Miller, C. A. Morgan, D. J. Kieber, D. W. King, J. A. Snow, B. G. Heikes, K. Mopper and J. J. Kiddle, Hydrogen Peroxide Method Intercomparision Study in Seawater, *Mar. Chem.*, 2005, **97**, 4-13.

16 C. A. Moore, C. T. Farmer and R. G. Zika, Influence of the Orinoco River on Hydrogen Peroxide Distribution and Production in the Eastern Caribbean, *J.Geophys. Res.*, 1993, **98**, 2289-2298.
17 D. Price, R. F. C. Mantoura and P. J. Worsfold, Shipboard Determination of Hydrogen Peroxide in the Western Mediterranean Sea using Flow Injection with Chemiluminescence Detection, *Anal. Chim. Acta.*, 1998, **371**, 205–215.
18 B. Palenik and F. M. M. Morel, Dark Production of H_20_2 in the Sargasso Sea, *Limnol. Oceanogr.*, 1988, **33**, 1606-1611.
19 G. Sarthou, C. Jeandel, L. Brisset, D. Amouroux, T. Besson and O. F. X. Donard, Fe and H_2O_2 Distributions in the Upper Water Column in the Indian Sector of the Southern Ocean, *Earth Planet. Sci. Lett.*, 1997, **147**, 83–92.
20 S. Steigenberger and P. L. Croot, Identifying the Processes Controlling the Distribution of H_2O_2 in Surface Waters Along a Meridional Transect in the Eastern Atlantic, *Geophys. Res. Lett.*, 2008, **35**, L03616, doi:10.1029/2007GL032555.
21 B. H. Yocis, *Dynamics of the Hydrogen Peroxide in Antartic Waters*, M.S. Thesis, State University of New York, College of Environmental Science and Forestry, 1995.
22 B. H. Yocis, D. J. Kieber and K. Mopper, Photochemical production of hydrogen peroxide in Antarctic waters, *Deep-Sea Res.*, 2000, **47,** 1077-1099.
23 J. Yuan and A. M. Shiller, The Distribution of Hydrogen Peroxide in the Southern and Central Atlantic Ocean, *Deep-Sea Res. II*, 2001, **48**, 2947–2970.
24 J. Yuan and A. M. Shiller, Hydrogen Peroxide in Deep Waters of the North Pacific Ocean, *Geophys. Res. Lett.*, 2004, **31**, L01310, doi:10.1029/2003GL018439.
25 J. Yuan and A. M. Shiller, Distribution of hydrogen peroxide in the northwest Pacific Ocean, *Geochem. Geophys. Geosys.*, 2010, **6**, Q09M02, doi:10.1029/2004GC000908.
26 R. G. Zika, J. W. Moffett, R. G. Petasne, W. J. Cooper and E. S. Saltzman, Spatial and Temporal Variations of Hydrogen Peroxide in Gulf of Mexico Waters, *Geochim. Cosmochim. Acta*, 1985, **49**, 1173-1184.
27 J. J. Morris, Z. I. Johnson, M. J. Szul, M. Keller and E. R. Zinser, Dependence of the Cyanobacterium *Prochlorococcus* on Hydrogen Peroxide Scavenging Microbes for Growth at the Ocean's Surface, *PLoS ONE*, 2011, **6**, e16805, doi:10.1371/journal.pone.0016805.
28 F. Leunert, W. Eckert, A. Paul, V. Gerhardt and H. –P. Grossart, Phytoplankton Response to UV-Generated Hydrogen Peroxide from Natural Organic Matter, *J. Plankton Res*., 2014, **36**, 185-197.
29 B. M. Voelker and B. Sulzberger, Effects of Fulvic Acid on Fe (II) Oxidation by Hydrogen Perxoide, *Environ. Sci. Technol.*, 1996, **30**, 1106-1114.
30 A. W. Vermilyea and B. Voelker, Photo-Fenton Reaction at Near Neutral pH, *Env. Sci. Technol.* 2009, **43***,* 6927–6933.
31 C. J. Miller, S. M. V. Lee, A. L. Rose and T. D. Waite, Impact of Natural Organic Matter on H_2O_2-Mediated Oxidation of Fe(II) in Coastal Seawaters, *Env. Sci. Techol.*, 2012, **46**, 11078−11085.
32 F. J. Millero and S. Sotolongo, The Oxidation of Fe(II) with H_2O_2 in Seawater, *Geochim. Cosmochim. Acta*, 1989, **53**, 1867-1873.
33 J. W. Moffett and R. G. Zika, Reaction Kinetics of Hydrogen Peroxide with Copper and Iron in Seawater, *Environ. Sci. Technol*., 1987, **21**, 804-810.

34 W. G. Sunda and S. A. Huntsman, Photoreduction of Manganese Oxides in Seawater and its Geochemical and Biological Implications, *Nature*, 1994, **301**, 234-236.

35 M. Gonzalez-Davila, J. M. Santana-Casiano and F. J. Millero, Oxidation of Iron(II) Nanomolar with H_2O_2 in Seawater, *Geochim. Cosmochim. Acta,* 2005, **69**, 83-93.

36 M. Pettine, F. Gennari, L. Campanella and F. J. Millero, The Effect of Organic Compounds in the Oxidation Kinetics of Cr(III) by H_2O_2, *Geochim. Cosmochim. Acta*, 2008, **72**, 5692–5707.

37 N. M. Scully and W. F. Vincent, Hydrogen Peroxide: A Natural Tracer of Stratification and Mixing Processes in Subartic Lakes. *Arch. Hydrobiol.*, 1997, **139**, 1-15.

38 N. M. Scully, W. F. Vincent, D. R. S. Lean and S. MacIntyre, Hydrogen Peroxide as a Natural Tracer of Mixing, *Aquatic Sci*., 1998, **60**, 169-186.

39 J. M. C. Plane, R. G. Zika, R. G. Zepp and L. A. Burns, Photochemical Modeling Applied to Natural Waters in *Photochemistry of Environmental Aquatic Systems*, ed. R. G. Zika and W. J. Cooper, American Chemical Society, Washington, D.C., 1987, pp 250-267.

40 J. W. Moffett and O. C. Zafiriou, An Investigation of Hydrogen Peroxide Chemistry in Surface Waters of Vineyard Sound with $H_2{}^{18}O_2$ and ${}^{18}O_2$, *Limnol. Oceanogr.*, 1990, **35**, 1221-1229.

41 R. G. Petasne and R. G. Zika, Hydrogen Peroxide Lifetimes in South Florida Coastal and Offshore Waters, *Mar. Chem*., 1987, **56,** 215-225.

42 J. W. Moffett and O. C. Zafiriou, The Photochemical Decomposition of Hydrogen Peroxide in Surface Waters of the Eastern Caribbean and Orinoco River, *J. Geophys. Res.*, 1993, **98**, 2307-231.

43 J. M. Diaz, C. M. Hansel, B. M. Voelker, C. M. Mendes, P. F. Andeer and T. Zhang, Widespread Production of Extracellular Superoxide by Heterotrophic Bacteria, *Science*, 2013, **340**, 1223-1226.

44 J.-A. Marshall, M. de Salas, T. Oda and G. Hallegraeff, Superoxide Production by Marine Microalgae, *Mar. Biol.*, 2005, **147**, 533–540.

45 B. Palenik, D. J. Kieber and F. M. M. Morel, Dissolved Organic Nitrogen Use by Phytoplankton: The Roll of Cell-Surface Enzymes, *Biol. Oceanogr*., 1992, **6**, 347-354.

46 A. L. Rose, A. Godrant, M. Furnas and T. D. Waite, Dynamics of Nonphotochemical Superoxide Production and Decay in the Great Barrier Reef Lagoon, *Limnol. Oceanogr.*, 2010, **55**, 1521–1536.

47 A. W. Vermilyea, S. P. Hansard and B. Voelker, Dark Production of Hydrogen Peroxide in the Gulf of Alaska, *Limnol. Oceanogr.*, 2010, **55**, 580–588.

48 R. Weller and O. Schrems, H_2O_2 in the Marine Troposphere and Seawater of the Atlantic Ocean (48 ^{o}N—63 ^{o}W), *Geophys. Res. Lett*., 1993, **20**, 125– 128.

49 W. J. Cooper, E. S. Saltzman and R. G. Zika, The Contribution of Rainwater to Variability in Surface Ocean Hydrogen Peroxide, *J. Geophys. Res.*, 1987, **92**, 2970–2980.

50 J. Yuan and A. M. Shiller, The Variation of Hydrogen Peroxide in Rainwater Over the South and Central Atlantic Ocean, *Atmos. Environ.*, 2000, **34**, 3973–3980.

51 N. V. Blough and R. G. Zepp, Reactive Oxygen Species in Natural Waters, in *Active Oxygen in Chemistry*, ed. C. S. Foote, J. S. Valentine, A. Greenberg and J. F. Liebman, Chapman and Hall, New York, NY, 1995, pp 280-333.

52 D. M. Karl and J. Resing, Palmer LTER: Hydrogen Peroxide in the Palmer LTER region: IV. Photochemical Interactions with Dissolved Organic Matter, *Ant. J. US*, 1993, **28**, 231-234.

53 Y. Zhang, R. Del Vecchio and N. V. Blough, Investigating the Mechanism of Hydrogen Peroxide Photoproduction by Humic Substances, *Environ. Sci. Technol.*, 2012, **46**, 11836-11844.

54 O. C. Zafiriou, Chemistry of Superoxide Ion-Radical (O_2^-) in Seawater. I. pK^*_{asw} (HOO) and Uncatalyzed Dismutation Kinetics Studied by Pulse Radiolysis, *Mar.Chem.*, 1990, **30**, 31-43

55 L. C. Powers and W. L. Miller, Blending Remote Sensing Data Products to Estimate Photochemical Production of Hydrogen Peroxide and Superoxide in the Surface Ocean, *Environ. Sci.: Process and Impacts*, 2014, 10.1039/C3EM00617D.

56 O. C. Zafiriou, B. M. Voelker and D. L. Sedlak, Chemistry of the Superoxide Radical (O_2^-) in Seawater: Reactions with Inorganic Copper Complexes, *J. Phys. Chem. A*, 1998, **102**, 5693-5700.

57 A. L. Rose, E. A. Webb, T. D. Waite and J. W. Moffett, Measurement and Implications of Nonphotochemically Generated Superoxide in the Equatorial Pacific, *Environ. Sci. Technol.*, 2008, **42**, 2387-2393.

58 S. P. Hansard, A. W. Vermilyea and B. M. Voelker, Measurements of Superoxide Radical Concentration and Decay Kinetics in the Gulf of Alaska, *Deep-Sea Res. I*, 2010, **57**, 1111-1119.

59 M. I. Heller and P. L. Croot, Superoxide Decay Kinetics in the Southern Ocean, *Environ. Sci. Technol.*, 2010, **44**, 191-196.

60 N. V. Blough, Photochemistry in the Sea-Surface Microlayer, in *The Sea Surface and Global Change*, ed. P. S. Liss and R. A. Duce, Cambridge University Press, Oxford, UK, 1997, pp 383-424.

61 D. W. O'Sullivan, P. J. Neale, R. B. Coffin, T. J. Boyd and C. L. Osburn, Photochemical Production of Hydrogen Peroxide and Methylhydroperoxide in Coastal Waters, *Mar. Chem.*, 2005, **97**, 14– 33.

62 R. J. Sikorski and R. G. Zika, Modeling Mixed-Layer Photochemistry of H_2O_2: Optical and Chemical Modeling of Production, *J. Geophys. Res.*, 1993, **98**, 2315-2328**.**

63 W. L. Miller and D. R. Kester, Hydrogen Peroxide Measurement in Seawater by (*p*-Hydroxyphenyl) Acetic Acid Dimerization, *Anal. Chem.*, 1988, **60**, 2711-2715.

64 D. A. Toole, D. J. Kieber, R. P. Kiene, D. A. Siegel and N. B. Nelson, Photolysis and the Dimethylsulfide (DMS) Summer Paradox in the Sargasso Sea, *Limnol. Oceanogr.*, 2003, **48**, 1088-1100.

65 M. Babin, D. Stramski, G. M. Ferrari, H. Claustre, A. Bricaud, G. Obolensky and N. Hoepffner, Variations in the light absorption coefficients of phytoplankton, nonalgal particles, and dissolved organic matter in coastal waters around Europe, *J. Geophys. Res.*, 2003, **108**, 3211, doi:10.1029/2001JC000882.

66 G. W. Miller, *Wavelength and Temperature-Dependent Apparent Quantum Yields for Photochemical Formation of Hydrogen Peroxide in Seawater*, M.S. Thesis, State University of New York, College of Environmental Science and Forestry, Syracuse, NY, 2000.

67 C. G. Hatchard and C. A. Parker, A New Sensitive Chemical Actinometer II. Potassium Ferrioxalate as a Standard Chemical Actinometer, *Proc. Royal Soc. of London Series A*, 1956, **235**, 518-536.

68 H. J. Kuhn, S. E. Braslavsky and R. Schmidt, Chemical Actinometry, *Pure Appl. Chem.*, 1989, **61**, 187-210.

69 E. M. White, D. J. Kieber, J. Sherrard, W. L. Miller and K. Mopper, Carbon Dioxide and Carbon Monoxide Photoproduction Quantum Yields in the Delaware Estuary, *Mar. Chem*., 2010, **118**, 11-21.

70 J. J. Cullen, P. J. Neale and M. P. Lesser, Biological Weighting Function for the Inhibition of Phytoplankton Photosynthesis by Ultraviolet Radiation, *Science*, 1992, **258**, 646-650.

71 P. J. Neale and J. J. Fritz, Experimental Exposure of Plankton Suspensions to Polychromatic Ultraviolet Radiation for Determination of Spectral Weighting Functions, in *Ultraviolet Ground- and Space-Based Measurements, Models, and Effects*, vol. 4482, ed. J. Slusser, J. R. Herman and W. Gao, SPIE-The International Society for Optical Engineering, San Diego, CA, 2001, pp 291– 296, http://dx.doi.org/10.1117/12.452930.

72 J. W. Verhoeven, Glossary of Terms used in Photochemistry, *Pure Appl. Chem.*, 1996, **68**, 2223-2286.

73 J. J. Jankowski, D. J. Kieber, K. Mopper and P. J. Neale, Development and intercalibration of ultraviolet solar actinometers, *Photochem. Photobiol.*, 2000, **71**, 431 – 440.

74 P. J. Neale, Spectra Weighting Functions for Quantifying the Effects of Ultraviolet Radiation in *Marine Ecosystems, in Effects of UV Radiation on the Marine Environment*, ed. S. J. de Mora, S. Demers and M. Vernet, Cambridge University Press, Oxford, UK, 2000, pp 73-100.

75 R. D. Rundel, Action Spectra and Estimation of Biologically Effective UV Radiation, *Physiol. Plant.*, 1983, **58**, 360-366.

76 D. J. Kieber, B. H. Yocis and K. Mopper, Free-Floating Drifter for Photochemical Studies in the Water Column, *Limnol. Oceanogr.*, 1997, **42**, 1829-1833.

78 R. Szymczak and T. D. Waite, Generation and Decay of Hydrogen Peroxide in Estuarine Waters, *Aust. J. Mar. Freshwater Res.*, 1988, **39**, 289-299.

79 S. S. Andrews, S. Caron and O. C. Zafiriou, Photochemical Oxygen Consumption in Marine Waters. A Major Sink for Colored Dissolved Organic Matter? *Limnol. Oceanogr.*, 2000, **45**, 267-277.

80 W. L. Miller, D. W. King , J. Lin and D. R. Kester, Photochemical Redox Cycling of Iron in Coastal Seawater, *Mar. Chem.*, 1995, **50**, 63-77.

81 N. M. Scully, D. J. McQueen, D. R. S. Lean and W. J. Cooper, Hydrogen Peroxide Formation: The Interaction of Ultraviolet Radiation and Dissolved Organic Carbon in Lakewaters Along a 43-75 ^{o}N Gradient, *Limnol. Oceanogr*., 1996, **41**, 540-548.

82 C. D. Clark , W. J. de Bruyn and J. G. Jones, Photochemical Production of Hydrogen Peroxide in Size-Fractionated Southern California Coastal Waters, *Chemosphere*, 2009, **76**, 141–146.

83 B. Herut, E. Shoham-Frider, N. Kress, U. Fiedler and D. L. Angel, Hydrogen Peroxide Production Rates in Clean and Polluted Coastal Marine Waters of the Mediterranean, Red and Baltic Seas, *Mar. Pollut. Bull.*, 1998, **36**, 994–1003.

84 R. Szymczak and T. D. Waite, Photochemical Activity in Waters of the Great Barrier Reef, *Estuar. Coast. Shelf Sci*.,1991, **33**, 605-622.

85 T. D. Waite and F. M. M. Morel, Photoreductive Dissolution of Colloidal Iron Oxides in Natural Waters, *Environ. Sci. Technol.*, 1984, **18**, 860-868.

86 S. P. Hansard, H. D. Easter and B. M. Voelker, Rapid Reaction of Nanomolar Mn(II) with Superoxide Radical in Seawater and Simulated Freshwater, *Environ. Sci. Technol.*, 2011, **45,** 2811–2817.

87 K. Wuttig, M. I. Heller and P. L. Croot, Reactivity of Inorganic Mn and Mn Desferrioxamine B with O_2, O_2^-, and H_2O_2 in Seawater, *Environ. Sci. Technol*., 2013, **47,** 10257−10265.
88 B. M. Voelker, D. L. Sedlak and O. C. Zafiriou, Chemistry of Superoxide Radical in Seawater: Reactions with Organic Cu Complexes, *Environ. Sci. Technol*., 2000, **34**, 1036-1042.
89 J. V. Goldstone and B. M. Voelker, Chemistry of Superoxide Radical in Seawater: CDOM Associated Sink of Superoxide in Coastal Waters, *Environ. Sci. Technol*., 2000, **34**, 1043-1048.
90 T. E. Thomas-Smith and N. V. Blough, Photoproduction of Hydrated Electron from Constituents of Natural Waters, *Environ. Sci. Technol*., 2001, **35**, 2721-2726.
91 S. Garg., A. L. Rose and T. D. Waite, Superoxide Mediated Reduction of Organically Complexed Iron(III): Comparison of Non-Dissociative and Dissociative Reduction Pathways, *Environ. Sci. Technol*., 2007, **4**1, 3205-3212.
92 D. A. Toole, D. J. Kieber, R. P. Kiene, E. E. White, J. Bisgrove, D. A. del Valle and D. Slezak, High Dimethylsulfide Photolysis Rates in Nitrate-Rich Antarctic Waters, *Geophys. Res. Lett.*, 2004, **31**, L11307, DOI: 10.1029/2004GL019863.
93 C. J. Deal, D. J. Kieber, D. A. Toole, K. Stamnes, S. Jiang and N. Uzuka, Dimethylsulfide Photolysis Rates and Apparent Quantum Yields in Bering Sea Seawater, *Cont. Shelf Res.*, 2005, **25**, 1825-1835.
94 P. S. Weiss, S. S. Andrews, J. E. Johnson and O. C. Zafiriou, Photoproduction of Carbonyl Sulfide in South Pacific Ocean Waters as a Function of Irradiation Wavelength, *Geophys. Res. Lett.,* 1995, **22**, 215-218
95 H. Aarnos, P. Ylöstalo and A. V. Vähätalo, Seasonal Phototransformation of Dissolved Organic Matter to Ammonium, Dissolved Inorganic Carbon, and Labile Substrates Supporting Bacterial Biomass Across the Baltic Sea. *J. Geophys. Res.*, 2012, **117**, G01004, doi:10.1029/2010JG001633.
96 R. J. Kieber, X. Zhou and K. Mopper, Formation of Carbonyl Compounds from UV-Induced Photodegradation of Humic Substances in Natural Waters: Fate of Riverine Carbon in the Sea, *Limnol. Oceanogr.*, 1990, **35**, 1503-1515.
97 S. C. Johannessen and W. L. Miller, Quantum Yield for the Photochemical Production of Dissolved Inorganic Carbon in Seawater, *Mar. Chem.*, 2001, **76**, 271–283.
98 C. G. Fichot and W. L. Miller, An Approach to Quantify Depth-Resolved Marine Photochemical Fluxes Using Remote Sensing: Application to Carbon Monoxide (CO) Photoproduction. *Remote Sens. Env.*, 2010, **114**, 1363-1377.
99 K. Mopper, X. Zhou, R. J. Kieber, D. J. Kieber, R. J. Sikorski and R. J. Jones, Photochemical Degradation of Dissolved Organic Carbon and its Impact on the Oceanic Carbon Cycle, *Nature*, 1991, **353**, 60-62.

926 Table 1. Activation energy for the photochemical production of hydrogen peroxide in seawater at
927 five wavelengths; the irradiation bandwidth was set at ± 5 nm for 290, 300 and 320 nm and ± 9.8
928 nm for 360 and 400 nm. The error for E_a denotes a 95% confidence interval.
929
930

	Activation Energy (E_a, kJ mol^{-1})				
Sample	**290 nm**	**300 nm**	**320 nm**	**360 nm**	**400 nm**
Booth Bay Harbor	12.4 ± 4.0	12.3 ± 2.2	15.6 ± 2.7	18.0 ± 3.8	24.0 ± 5.7
Rhode River estuary	19.2 ± 2.2	15.9 ± 2.0	17.7 ± 2.8	21.7 ± 5.4	26.2 ± 8.1
Hawaii Station ALOHA	21.7 ± 3.3	20.4 ± 3.1	23.3 ± 3.0	24.9 ± 6.4	34.1 ± 12.2
Antarctic Station B	9.6 ± 2.3	8.3 ± 2.6	13.6 ± 3.6	21.7 ± 26.0	20.8 ± 48.8
Antarctic Station N	16.9 ± 3.7	21.1 ± 3.6	22.5 ± 6.3	28.9 ± 13.4	33.5 ± 9.4
Arthur Harbor, Palmer Station	19.7 ± 2.2	28.7 ± 3.5	35.2 ±12.8	42.1 ± 15.3	52.7 ± 9.7

931
932

Table 2. Total daytime, depth-integrated photochemical production rate for H_2O_2 in seawater determined from free-floating drifter studies conducted at Ammen Rock and the Damariscotta River outflow in the Gulf of Maine, and at Station E in the northwest Atlantic Ocean. The reported error is the standard deviation for measured and modeled rates. Modeled rate could not be determined (ND) at Station E because measured irradiance data were not available at this station.

Station	Sampling Depth (m)	Depth-Integrated Production (mmol m^{-2} d^{-1}) Measured	Modeled	% Difference
Ammen Rock	15	1.10 ± 0.025	0.96 ± 0.028	9.4
Damariscotta River outflow	15	0.68 ± 0.016	0.58 ± 0.020	14.0
Station E (NW Atlantic Ocean)	20	0.77 ± 0.012	ND	ND

946 **FIGURES**

947

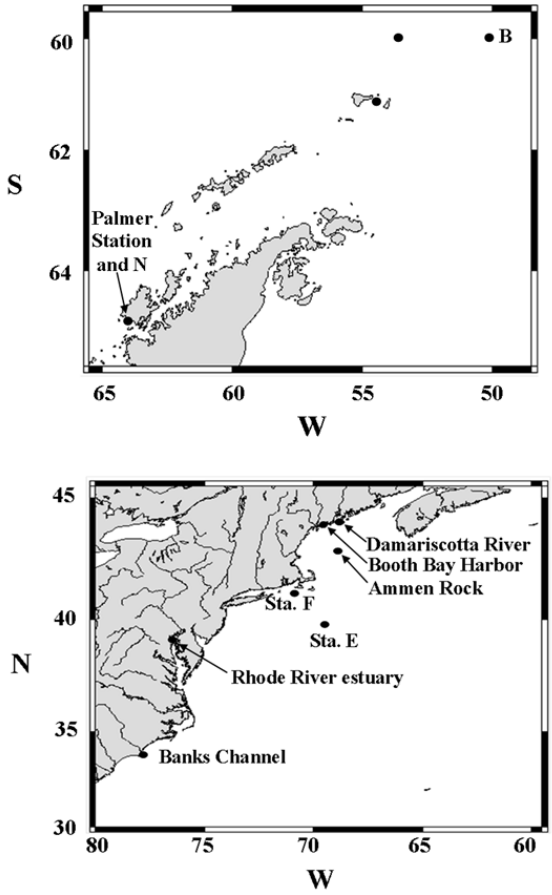

948

949 **Figure 1**. Location of hydrographic stations in (A) the confluence of the Weddell and Scotia
950 Seas, and the Antarctic Peninsula; and (B) along the East Coast of the United States. Not shown
951 are Hawaii Station ALOHA and the Gulf of Mexico station.

952

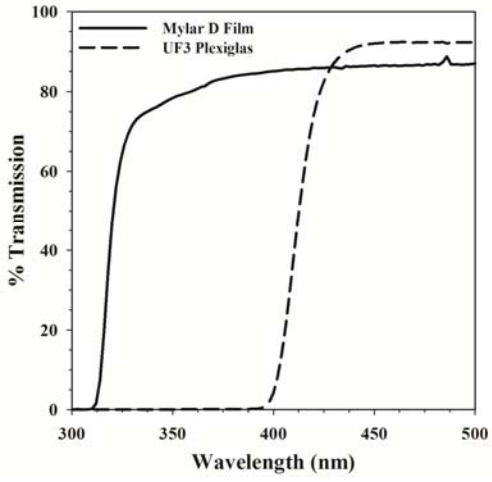

953

954

955 **Figure 2**. Transmission spectra for Mylar D polyester film and UF3 Plexiglas.

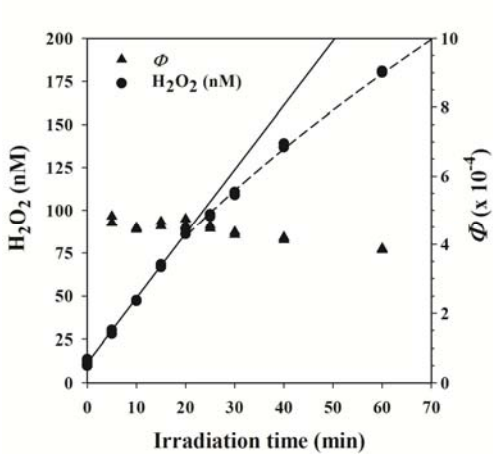

Figure 3. Photochemical formation of hydrogen peroxide in 0.2 μm-filtered Ammen Rock, Gulf of Maine seawater and the apparent quantum yield as a function of irradiation time at 300 ± 5 nm. Apparent quantum yields were corrected to account for losses in absorbance observed for longer irradiations. The solid line is the best-fit line of the production data as determined from linear regression analysis, excluding data from 25-60 min. The dashed line is the best-fit line determined from non-linear regression analysis.

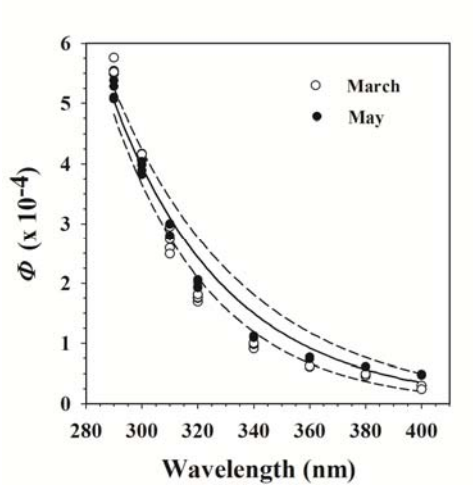

Figure 4. Comparison of wavelength-dependent apparent quantum yields in freshly collected Rhode River estuary water determined with narrow bandwidth (○) and polychromatic irradiation systems (solid line). The dashed lines denote the upper and lower 95% confidence interval for the polychromatic study. The narrow bandwidth experiment was repeated 2.5 months later with stored (4 °C) 0.2 μm-filtered Rhode River estuary water (●). All apparent quantum yields were determined at 9 °C.

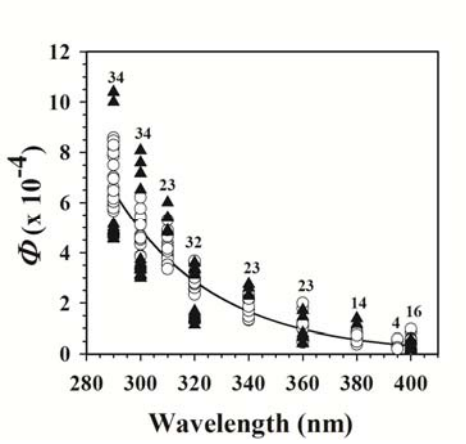

Figure 5. (A) Wavelength-dependent apparent quantum yields for the photochemical formation of hydrogen peroxide in nine marine waters at 25 °C with low (< 0.5 m^{-1}, ▲) or high (> 0.7 m^{-1}, ○) DOM absorption coefficients at 300 nm. The best-fit line was determined from non-linear regression analysis. Data shown in this figure are tabulated in Miller (2000)[66]. The value of n above each data set represents the total number of samples analyzed at that wavelength.

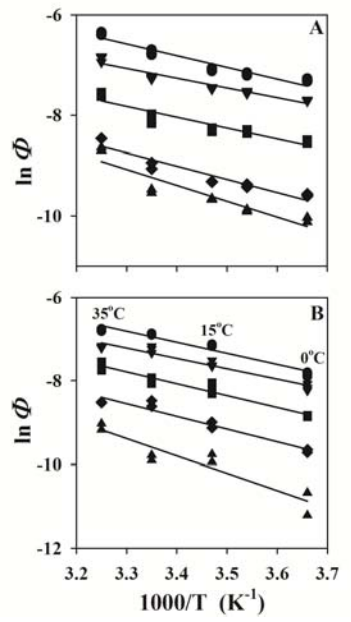

Figure 6. Natural logarithm of the apparent quantum yield plotted as a function of inverse temperature for 0.2 μm-filtered (A) Rhode River estuary water and (B) Hawaii Station ALOHA seawater. The activation energy was determined from the slope of the best-fit line determined from linear regression analysis of the data at (●) 290, (▼) 300, (■) 320, (♦) 360 and (▲) 400 nm. Three irradiation temperatures are listed in Panel B above the 290 nm data set.

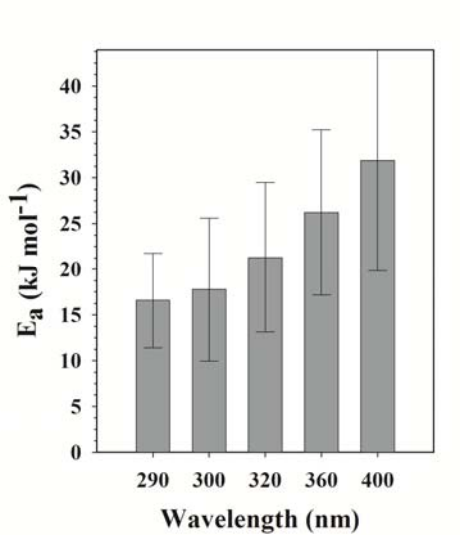

Figure 7. Average activation energy for the data shown in Table1 plotted as a function of wavelength. Error bars denote the 95% confidence interval.

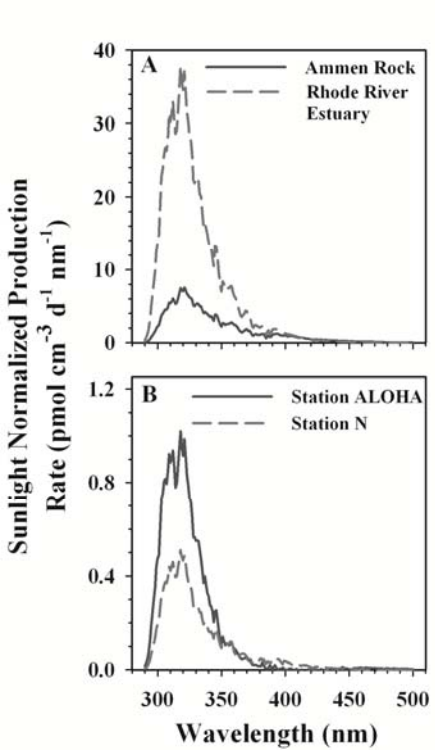

Figure 8. Sunlight normalized production rates for hydrogen peroxide at the sea surface in (A) coastal seawater and (B) oligotrophic seawater. Note the y-axis scale change in panels A and B.

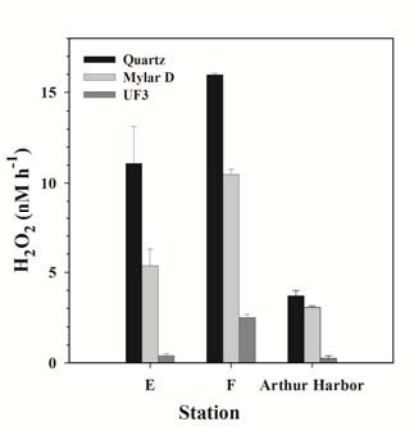

Figure 9. Hydrogen peroxide photochemical production rates in 0.2 μm-filtered seawater samples, collected from the northwest Atlantic Ocean stations E and F, and Arthur Harbor, Palmer Station, Antarctica, that were exposed to sunlight in quartz tubes or quartz tubes enclosed with long-pass filters, Mylar D or UF3 Plexiglas. Error bars denote the standard deviation of four replicates.

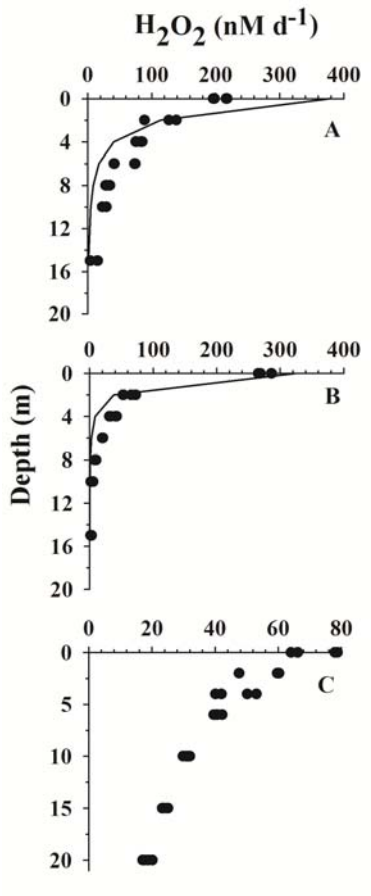

Figure 10. Hydrogen peroxide photochemical production rates as a function of depth determined from a free-floating drifter study (●) and predicted from a photochemical model (–) for (A) Ammen Rock, Gulf of Maine and (B) the Damariscotta River outflow, Gulf of Maine. (C) Hydrogen peroxide photochemical production rates as a function of depth determined from a floating drifter study in the northwest Atlantic Ocean, Station E. Production rates were not modeled at Station E, since measured spectral photon exposure data were not available for this station.